Article

Versatile Barometer Biosensor Based on Au@Pt Core/shell Nanoparticle Probe

Qiangqiang Fu, Ze Wu, Dan Du, Chengzhou Zhu, Yuehe Lin, and Yong Tang

ACS Sens., **Just Accepted Manuscript** • Publication Date (Web): 01 Jun 2017

Versatile Barometer Biosensor Based on Au@Pt Core/shell Nanoparticle Probe

Qiangqiang Fu[a, b], Ze Wu[a], Dan Du[b], Chengzhou Zhu [b], Yuehe Lin[b]*, Yong Tang[a, c]*

[a] Guangdong Province Key Laboratory of Molecular Immunology and Antibody Engineering, Jinan University, Guangzhou 510632, PR China.

[b] School of Mechanical and Materials Engineering, Washington State University, Pullman, WA 99164, USA.

[c] Institute of Food Safety and Nutrition, Jinan University, Guangzhou, 510632, PR China.

KEYWORDS: *Barometer-based biosensors, core-shell Au@Pt nanoparticles, Nanocatalysts, Immune-sensors; Aptasensors*

ABSTRACT: There is a high global demand for sensitive, portable, user-friendly, and cost-effective biosensors. In this work, we introduce a barometer-based biosensor for the detection of a broad range of targets. The device is operated by measuring the pressure change produced by oxygen (O_2) generation in a limited chamber using a portable barometer. The design employs core-shell Au@Pt nanoparticles (Au@PtNPs) as the bioassay probe to catalyze the decomposition of H_2O_2 and the release of O_2. As a proof of concept, we developed barometer-based immune-sensors to detect carcinoembryonic antigen (CEA) and ractopamine (Rac). In addition, barometer-based aptasensors for sensitive detection of thrombin and mercury ion (Hg^{2+}) were also developed. In order to facilitate the analysis of results, we have developed a smartphone software to calculate, save and wirelessly trsnsmit the results. Linear detection ranges for detection of CEA, Rac, thrombin and Hg^{2+} were 0.025 ng/mL-1.6 ng/mL, 0.0625 ng/mL-4 ng/mL, 4 U/L-128 U/L and 0.25 ng/mL-16 ng/mL, respectively. The detection limit of these four analytes is 0.021 ng/mL, 0.051 ng/mL, 2.4 U/L and 0.22 ng/mL, respectively. Furthermore, the developed barometer-based biosensors exhibited high specificities for these four analytes. CEA in serum samples, Rac in urine samples, thrombin in serum samples and Hg^{2+} in river water samples were measured by the barometer-based biosensors. Obtained results of these targets from barometer-based biosensors were consistent with detection results from traditional methods, indicating that barometer-based biosensors are widely applicable.

Despite the large demand for highly sensitive, highly selective, low cost, and portable biosensors, [1-3] current techniques have not been able to meet all of these criteria. There exist many well-developed methods and techniques that can achieve highly accurate and sensitive detection, including mass spectrometry, [4] quartz crystal microbalance sensors, [5-7] electrochemical sensors, [8-9] chemiluminescence sensors, [10-11] biochips, [12-13] enzyme-linked immunosorbent assays (ELISA), [14] nano-electrochemical sensors and DNA nano-electrochemical sensors, [15-16] and others methods. [17-25] However, most of these approaches require expensive and complicated instrumentation, high maintenance, high operating costs and professional operators. Because of these factors, these techniques have not been widely used in field testing in places with limited resources. In recent years, considerable effort has been devoted to developing on-site detection devices. [26-27] Lateral flow sensors are the most widely used field testing devices. [28] For example, Au nanoparticles (NPs) lateral flow sensors have been employed because of their portability, cost-effectiveness and the ability to visualize the results with naked eye. [29-31] Lateral flow sensors are highly sensitive when coupled with high-efficiency tracers, such as fluorescence NPs, [32-34] quantum dots, [35-36] and coded surface-enhanced Raman scattering (SERS) NPs. [37-40] However, a significant disadvantage of lateral flow sensors is that they require expensive readout instruments to produce quantitative results. Another technology widely used in field testing is microfluidic chips. [41-43] Qin' group[44] reported an elegant multiplexed volumetric microfluidic chip allowing direct visual quantification of target biomarkers without additional instrumentation. This type of microfluidic chip has been employed to test a variety of analytical targets. [45-46] Although the volumetric bar-chart chip requires a minimal number of accessory devices, the processing costs of the chip are high, and the microfluidic platform still requires a fluid-introducing accessory device and a pump control system. [47] In addition, the readout results of current volumetric microfluidic chips were ink-movement lengths, rather than concentration of analytes. A series of calculations was required. This problem has become an obstacle for extensive use of these biosensors by non-professional operators or untrained users.

In this study, we have developed a lower cost, portable and user-friendly barometer biosensor that enables quantitative detection of a broad range of analytes. The design employs core/shell Au@PtNPs as probes, which demonstrate excellent catalytic stability and high catalytic activity in the decomposition of H_2O_2 to release O_2. The generated O_2 accumulates within the limited volume chamber and causes an increase in pressure, which is measured by a portable barometer. The analyte concentrations are linearly proportional to the measured pressures. As a proof of concept, we developed barometer-based immune-sensors to detect CEA in serum samples and Rac in urine samples. In addition, we developed aptasensors to detect thrombin in serum samples and Hg^{2+} ion

in water samples. These results indicate that the barometer-based biosensors developed in this study have a wide range of applications.

METHODS AND MATERIALS

Materials and reagents

This section was presented in Supporting Information

Preparation of Au@PtNPs. The Au@PtNPs were synthesized according to previous reports.[48] For the preparation of AuNPs, 4 mL of 1% $HAuCl_4$ solution and 96 mL of ultrapure water were added to a round-bottom flask under a reflux condenser, and then headed the solution to boiling with magnetic stirring. Then, 3 mL of 4% sodium citrate was added, and the solution was keep boiled with stirring for 20 min. A wine-red liquid was obtained, indicating the formation of AuNPs. For the preparation of Au@PtNPs, 10 mL of AuNPs and 200 μL of 3.86 mM H_2PtCl_6 were mixed together，and then heated the mixture to 80 ℃ under magnetic stirring. 800 μL aliquot of 10 mM ascorbic acid was slowly added in this solution with 3 min. The mixture was then heated and stirred for another 30 min.

Preparation of Anti-CEA-antibody labeled magnetic beads (mAb1-MBs). MBs (100 μL) were washed by 1 mL washing buffer, and then suspended in 1 mL of PBS buffer. Then using 100 mM MES buffer (pH 4.8) diluted mAb1 to 1 mg/mL, and following mixed with the MBs. After 2 h, 100 μL of 10% BSA were added to block the surface of the MBs. After 1 h, the unconjugated mAb1 were removed under a magnetic rack. The resulting mAb1-MBs were resuspended into 100 μL PBS, and then stored at 4 ℃.

Barometer-based immune-sensors for detection of CEA. 5 μL mAb1-MBs were mixed 100 μL CEA samples. After 0.5 h, centrifuge tubes were placed in the magnetic rack with 3 min, and the mAb1-MBs were collected. After repeating this washing process 3 times, the MBs were resuspended in 100 μL of PBS. Then 4 μL mAb-Au@PtNPs mixed with mAb1-MBs with 30 min. After washing 5 times with PBST buffer, the mixtures were washed 5 times by PBST buffer and resuspended in 300 μL of 10 M H_2O_2. After 30 min, the barometric pressure within the tubes was measured by the barometer.

Detection of CEA in real serum samples. 5 μL of mAb1-MBs were transferred into 100 μL serum sample. After 0.5 h, the centrifuge tube was placed in a magnetic rack with 3 min, and then collected mAb1-MBs. After washing 3 times, mAb1-MBs were suspended into 100 μL of PBS, and then 4 μL of mAb-Au@PtNPs was mixed. After washing five times, the mixtures were resuspended in 300 μL 10 M H_2O_2. 30 min later, the barometric pressure in centrifuge tube was measured by the barometer.

For methods for detection of Rac, thrombin and Hg^{2+}, experimental process was displayed in Supporting Information.

RESULTS AND DISCUSSION

Design of the barometer bio-sensor. The principle of the barometer-based biosensor is displayed in Figure 1. The biosensor was assembled with a portable barometer, two valves, a silicone plug, and an Eppendorf tube (with a maximum capacity of 500 μL). These components were connected through three silicone tubes (with a diameter of 1 mm) and sealed with sealant. When the bio-reaction was completed, 300 μL of H_2O_2 were added into the tube, and a silicone plug was inserted into the tube at the 400 μL-mark. Valve A was then shut off, and after 1 min, valve B was shut off. After 30 min, the barometer was turned on and the reset button was pressed to display a pressure reading of 0 Pa. Subsequently, valve A was opened, and the pressure in the chamber was measured by the barometer. When the measurement was finished, valve B was opened, and the silicone plugs were removed from the tube. Furthermore, we have developed a smart phone software which was used to calculate, save and wirelessly transmit the results (Figure S4).

Characterization of the barometer-based biosensors. In this work, the barometric biosensor was operated by measuring the pressure change produced by oxygen (O_2) generation in a sealed chamber using a portable barometer. To sealed reaction chamber, plastic centrifuge tube was selected, rather than commonly used microwells. In experimentation, many washing steps were needed, and therefore MBs were used to conjugate with antibody, antigen or aptamer to prevent these bio-recognition elements from being washed out. To ensure sensitivity and stability of the barometer-based biosensor, an efficient and stable catalyst is needed to decompose H_2O_2 and generate O_2. Catalase is the most efficient natural enzyme, and nanomaterials containing group VIII metal elements have been reported that could catalytically decompose H_2O_2 to generate O_2. The order of activity decreasing in the sequence of Pt > Ir > Pd > Ru > Rh. [49] Therefore, they have been intensely applied.[50-53] In this study, Au@PtNPs were synthesized via

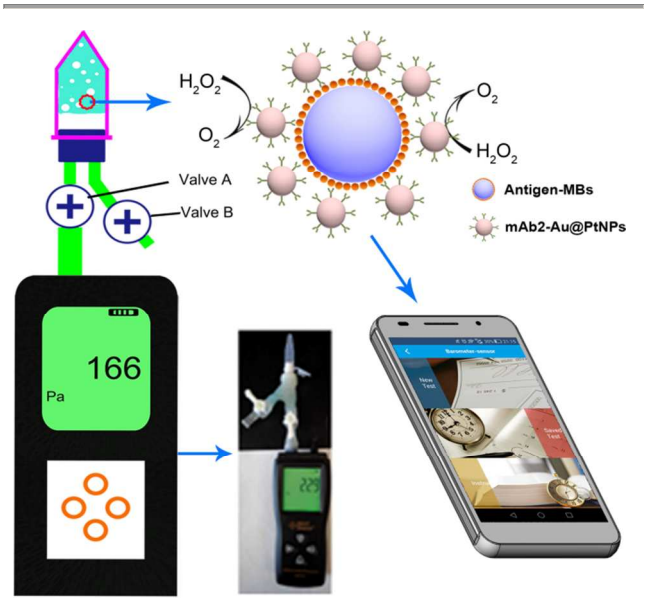

Figure 1. Scheme of the barometer-based biosensor. This barometer-based biosensor operates based on the measurement of oxygen generation in a limited chamber by using a precise barometer. The design employs Au@PtNPs as probes for the decomposition of H_2O_2 to release O_2. The generated O_2 accumulates within the limited volume chamber and causes an increase in pressure, which is measured by a portable barometer. Analyte concentrations are linearly proportional to the measured pressures.

deposition of a thin Pt layer on the surface of AuNPs. AuNPs exhibited a smooth surface and a diameter of 15 nm (Figure 2a). The Au@PtNPs exhibited a dendritic surface and a diameter of 21 nm (Figure 2b), and the absorption peak of Au@PtNPs was 510 nm (Figure 2c). These results are consistent with previous studies,[54-55] indicating the successful synthesis of Au@PtNPs. The catalytic efficiency of catalase and mAb2-Au@PtNPs was compared. The concentration of H_2O_2 may affect the catalytic efficiency of the catalyst. Catalase and mAb2-Au@PtNPs (at a final concentration of 3 pM) were diluted into different concentrations of H_2O_2 to generate O_2. With increasing H_2O_2 concentration, the released O_2 increased, reaching maximal activity levels at H_2O_2 concentration was 10 M (Figure 2d). Catalase exhibited maximal catalytic activity at an H_2O_2 concentration of 10 mM (Figure 2e). This result is consistent with previous studies[56]. Under optimal conditions, Au@PtNPs produce more O_2, indicating that Au@PtNPs were an efficient catalyst for the generation of O_2. The same concentration of catalase and Au@PtNPs reacted with BSA-Rac-MBs and, after washing, pressures were measured by barometer. The obtained pressure using Au@PtNPs was much higher than obtained pressure using catalase (Figure S1), indicating that Au@PtNPs is a preferred catalyst in barometer-based biosensors. The volume of the gas chamber of the barometer-based biosensor is approximately 200 μL. To yield a pressure change of 1 Pa in the chamber, approximately 2×10^{-3} μL of O_2 is needed. Since the molecular weight of the catalase used in this study was 250,000 KDa and the enzyme activity was 50,000 U/mg, 1.3×10^{-13} M of catalase was required to achieve the above pressure change under optimal conditions. Because the released O_2 of the mAb-Au@PtNPs was approximately 20 times that of catalase, 6.5×10^{-15} M of mAb-Au@PtNPs is theoretically required to produce a pressure change of 1 Pa. In our study, 40 fM of mAb-Au@PtNPs produced a pressure change of 181 Pa (Figure 2f). This value was close to the theoretical value. Furthermore, the Au@PtNPs also exhibited thermal stability. The Au@PtNPs retained 95% activity over 50 days at 4°C (Figure S2), whereas catalase lost 80% activity over 7 days at 4°C (Figure S3). Additionally, the mAb-Au@PtNPs preparation does not require laborious and costly purification steps to remove unconjugated mAb, unlike the preparation of mAb-catalase. Therefore, Au@PtNPs was selected. To assess the stability of the devices, different concentrations of mAb2-Au@PtNPs were used to generate O_2. In the first study, one barometer-based biosensor was used to measure barometric pressures from three independent experiments. The acquired values were approximately equivalent (Figure 2g, blue group). Second, barometric pressures were measured by three individual barometer-based bio-sensors simultaneously. There were no significant differences in the results from each biosensor (Figure 2g, red group), indicating the high stability of the barometer-based bio-sensors.

Detection of CEA using the barometer-based immune-sensor. CEA is usually present low concentration in healthy blood. However, the CEA concentration was increased in some cancer, especially cancers of the large intestine (colon and rectal cancer). In an adult non-smoker, the normal level of CEA is <2.5 ng/mL, and in a smoker, the normal level of CEA is <5.0 ng/mL.[57] For the sandwich immune-sensor, a capturing

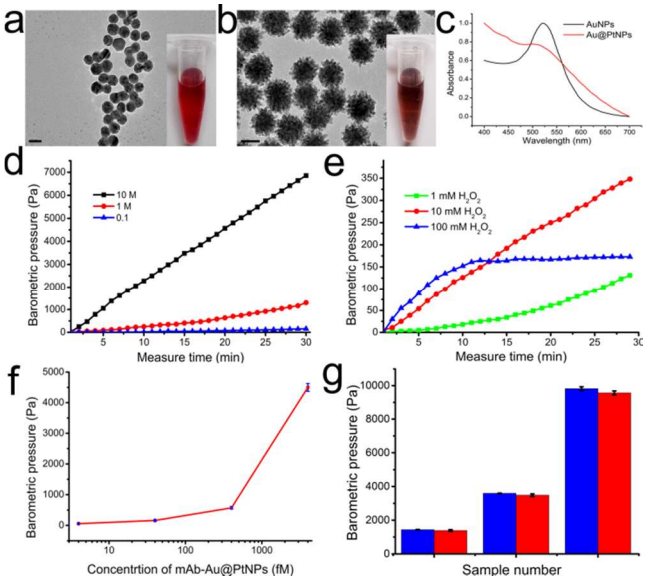

Figure 2. a-b. TEM images of the AuNPs and Au@PtNPs. Scale bar was 20 nm. **c**. Absorption spectra of the AuNPs and Au@PtNPs. **d**. Catalytic efficiency of mAb2-Au@PtNPs under different concentrations of H_2O_2. **e**. Catalytic efficiency of catalase under different concentrations of H_2O_2. **f**. Catalytic efficiency of different concentrations mAb2-Au@PtNPs under 10 M of H_2O_2. **g**. Stability of the barometer-based biosensor. Blue group shows the stability of a single barometer-based biosensor (3 measurements), and red group shows the stability of three barometer-based biosensors.

antibody was conjugated with MBs (mAb1-MBs), and mAb2 was conjugated with Au@PtNPs (mAb2-Au@PtNPs). For detect low concentrations CEA samples, the amount of mAb2-Au@PtNPs bound to mAb1-MBs was small. Because fewer H_2O_2 molecules were decomposed by the mAb-Au@PtNPs, the measured barometric pressures were low. For detect high concentrations CEA samples, a large number of mAb2-Au@PtNPs were bound to the mAb1-MBs. Therefore, the measured barometric pressures were high (Figure 3 a-b). In the CEA detection, a good linear correlation (R^2=0.994) was obtained between barometric pressure and CEA concentration within the range of 0.025 - 1.6 ng/mL (Figure 3c), and the limit of detection (LOD) was 0.021 ng/mL. To evaluate the specificity of the barometer-based CEA immune-sensor, the device was used to measure 1.6 ng/mL solutions of various proteins, and results showed high specificity (Figure 3d). CEA concentrations in serum samples were measured using the barometer-based immune-sensor and also separately by chemiluminescence immunoassay. The results from the barometer-based immune-sensor were correlated with those from chemiluminescence immunoassay (Figure 3e), indicating that the developed barometer-based immune-sensor could detect CEA in serum samples.

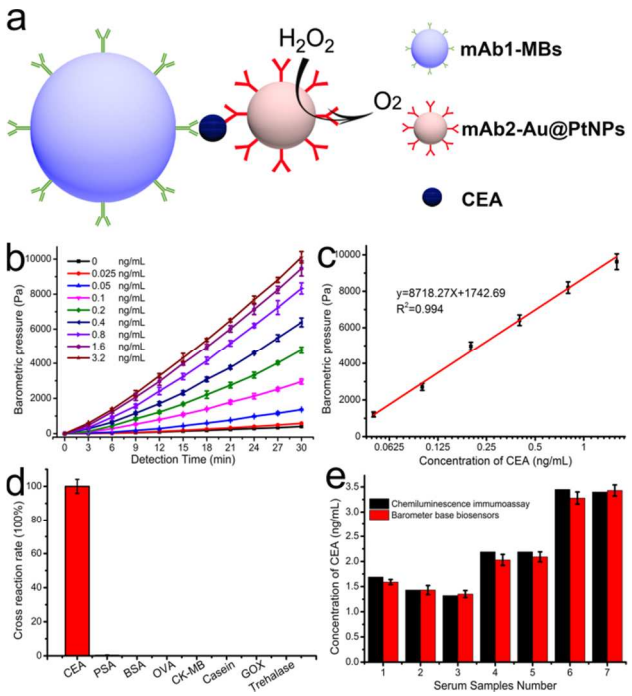

Figure 3. CEA detection using the barometer-based immune-sensor; **a.** Scheme of the barometric pressures for CEA detection; **b**. Concentration-dependent barometric pressures for the detection of CEA; **c.** Calibration curve of barometer-based immune-sensor for CEA detection; **d.** Specificity of the barometer-based immune-sensor for CEA detection. **e.** Comparison of CEA detection in serum samples using the barometer-based immune-sensor and chemiluminescence immunoassay.

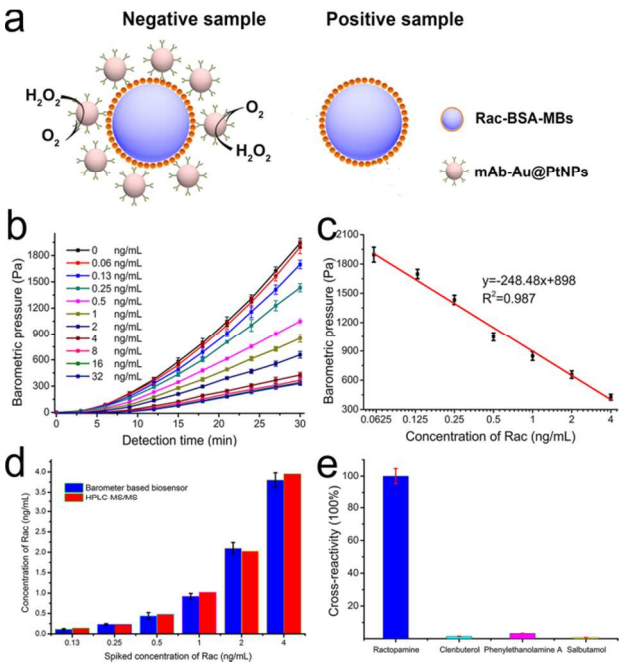

Figure 4. Rac detection using the barometer-based immune-sensor; **a.** Scheme of the barometer-based immune-sensor for the detection of Rac. **b.** Concentration-dependent barometric pressures for the detection of Rac; **c.** Calibration curve of barometer-based immune-sensor for Rac detection; **d.** Detection of Rac in urine samples using the barometer-based immune-sensor and HPLC-MS/MS; **e.** Specificity of the barometer-based immune-sensor for Rac detection.

Detection of ractopamine (Rac) using the barometer-based immune-sensor. Ractopamine (Rac) is a small bronchodilator molecule that often used as a selective agonist/antagonist. Ingestion of Rac may cause cardiac hypertrophy, irregular rhythms, and specific cell death. [58] For the Rac competitive immune-sensor, coating antigen Rac-BSA was conjugated with MBs, and an anti-Rac-mAb was labeled with Au@PtNPs to form mAb-Au@PtNPs. For the detection of low concentration Rac samples, the Au@PtNPs bound to the Rac-BSA-MBs, resulting in the production of O_2. Therefore, high pressures were measured. For the detection of positive samples, some of the mAb-Au@PtNPs bound to Rac, thus decreasing the amount of mAb-Au@PtNPs that bound to the Rac-BSA-MBs. Because fewer H_2O_2 molecules were decomposed by the mAb-Au@PtNPs, the measured barometric pressures were low (Figure 4a-b). In our Rac detection studies, a linear correlation (R^2=0.987) was obtained between barometric pressure and Rac concentration within 0.0625 ng/mL-4 ng/mL (Figure 4c), and the LOD was 0.051 ng/mL. To evaluate the specificity of the barometer-based Rac immune-sensor, the device was used to measure 4 ng/mL solutions of various agonists (clenbuterol, phenylethanolamine A, and salbutamol). The negligible cross-reaction rates for these agonists (1.5%, 3.34%, and 0.72%, respectively) indicated that the barometer-based immune-sensor had high specificity (Figure 4e). Rac was spiked into urine samples with different concentrations and then measured using the barometer-based immune-sensor and also separately by MS-MS-UPLC. The results from the barometer-based immune-sensor were correlated with those from MS-MS-UPLC (Figure 4d), indicating that the developed barometer-based immune-sensor could be used for food safety monitoring.

Detection of thrombin using the barometer-based aptasensor. Aptamers are selected from random oligonucleotide pools by a technique called systematic evolution of ligands by exponential enrichment (SELEX) and have the ability to bind a series of targets.[59] Compared with antibodies, aptamers are more easily synthesized and have stronger stability than antibodies. Therefore, aptamers have applied in many fields. In order to prove that our developed barometer-based biosensor could serve as an aptasensor, thrombin and mercury ions (Hg^{2+}) were tested.

Thrombin is a biomarker for cardiovascular disease and a crucial tumor marker for diagnosis of pulmonary metastasis. [60] In the sandwich aptasensor for detection of thrombin, aptamer 1 (T29) was conjugated with MBs and aptamer 2 (T15) was labeled with Au@PtNPs (T15-Au@PtNPs). For the detection of low concentrations thrombin samples, a small amount of T15-Au@PtNPs that bound to the T29-MBs. Because fewer H_2O_2 were decomposed by the T15-Au@-PtNPs, the measured barometric pressures were low. For the detection of serum samples with high concentration thrombin, a large number of T15-Au@PtNPs was bound to the T29-MBs. Therefore, the measured barometric pressures were high (Figure 5 a-b). In

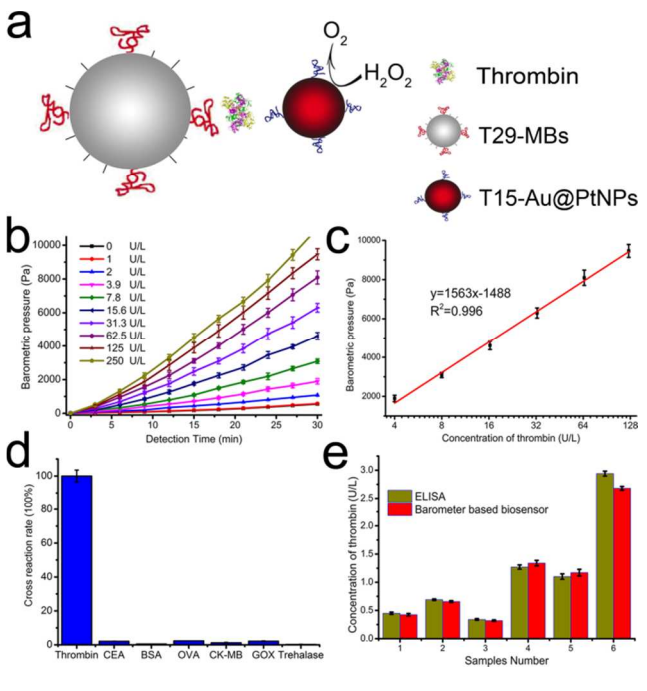

Figure 5. Thrombin detection using the barometer-based aptasensor; **a.** Scheme of the barometer-based aptasensor for detection of thrombin. **b.** Concentration-dependent barometric pressures for thrombin detection; **c.** The calibration curve of thrombin detection; **d.** Specificity of the barometer-based aptasensor for thrombin. **e.** Detection of thrombin in serum samples using the barometer-based aptasensor and ELISA. Amptamers in this study have the following sequences: T15 (5'-biotin-GGTTGGTGTGGTTGG-3'); T29 (5'-AGTCCGTG GTAGGGCAGGTTGGGGTGACT-biotin-3'). [61]

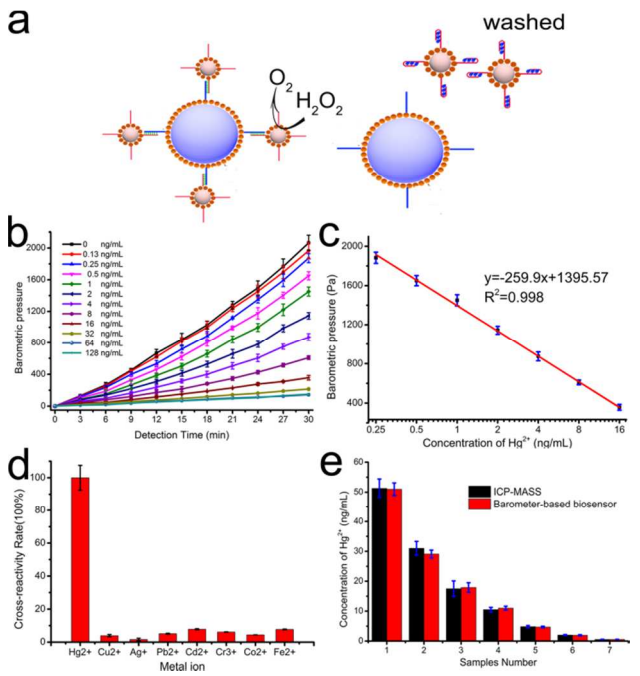

Figure 6. Hg^{2+} detection using the barometer-based aptasensor; **a.** Scheme of the barometer-based aptasensor for detection of Hg^{2+}. **b**. Concentration-dependent barometric pressures for the detection of Hg^{2+}; **c.** Calibration curve for Hg^{2+} detection; **d.** Specificity of the barometer-based aptasensor for Hg^{2+} detection. **e.** Detection of Hg^{2+} in water samples using the barometer-based aptasensor and ICP-MASS. Aptamers in this study have the following sequences: Mercury ion recognition aptamer (5'-biotin-AAAAAAAAAATTCTTTCTTCCCCTT GTTTGTT-3') and its complementary oligonucleotide (5'-biotin-AAAAAAAAAACACAAACAAGGCCAA CA-3'). [62]

thrombin detection studies, a good linear correlation (R^2=0.996) was obtained between barometric pressure and thrombin concentration within the range of 4-128 U/L (Figure 5c), and the LOD was 2.51 U/L. To evaluate the specificity of the barometer-based thrombin aptasensor, the device was used to measure 128 U/L solutions of various proteins, and results showed high specificity (Figure 5d). Thrombin concentrations in serum samples were measured using the barometer-based aptasensor and also separately by ELISA. The results from the barometer-based aptasensor were correlated with those from ELISA (Figure 5e), indicating that the developed barometer-based aptasensor may be used for detection of thrombin in serum samples.

Hg^{2+} detection using the barometer-based aptasensor. There is a great need for simple, reliable on-site analyses for Hg^{2+} in surface water, due to mercury accumulation in the body leads to brain and liver damage. In the competitive aptasensor, anti-Hg^{2+} aptamer was conjugated with Au@PtNPs (aptamer-Au@PtNPs). Also, MBs were labeled with complementary chains of aptamer (CC-MBs). For the detection of low concentrations Hg^{2+}samples, a large number of aptamer-Au@PtNPs was bound to the CC-MBs. Therefore, high barometric pressures were measured. For the detection of high concentration Hg^{2+} samples, the aptamer was bound with Hg^{2+} and furthermore could not bind with CC-MBs. Because fewer H_2O_2 molecules were decomposed by the Au@PtNPs, the measured barometric pressures were low (Figure 6a-b). In the Hg^{2+} detection, a good linear correlation (R^2=0.998) was obtained between barometric pressure and Hg^{2+} concentration within the range of 0.25-16 ng/mL (Figure 6c), and the LOD was 0.22 ng/mL. To evaluate the specificity of the barometer-based Hg^{2+} aptasensor, the device was used to measure16 ng/mL solutions of various ions. The negligible cross-reaction rates indicating that the barometer-based aptasensor had high specificity (Figure 6d). Hg^{2+} was spiked into river water samples with different concentrations and then measured using the barometer-based aptasensor and also separately by ICP-MS. The results from the barometer-based aptasensor were correlated with those from ICP-MS (Figure 6e), indicating that the developed barometer-based aptasensor may be used for environmental pollution monitoring.

Comparison of barometer-based biosensors and other methods. The detection results of the barometer-based biosensors for CEA, Rac, thrombin and Hg^{2+} were compared with those of other analytical technologies reported in the literature (Table S1). Although some of these techniques are more sensitive and accurate, the reported barometer biosensors do not need expensive instruments to obtain results, such as microplate reader, chemiluminescence analyzer and electrochemical workstation. Therefore, we believe that barometer-based biosensors are more suitable for some areas with limited resources because of their portability and cost-effectiveness.

CONCLUSIONS

In this study, we have developed a low-cost, portable, and user-friendly barometer-based biosensor. The developed barometer-based biosensor has many advantages. First, the barometer-based biosensor is free from expensive optical and electronic components. This advantage simplifies instrumental design and cost. Second, the experiment was more user-friendly, as the addition of the sample and the washing steps were completed in eppendorf tubes. Third, through the assistance of the smartphone software developed in this work, the users can easily get the concentration of the analytes and can save or transmit the results wirelessly. We developed barometer-based biosensors to detect CEA, Rac, thrombin and Hg^{2+}. Good performances of these biosensors indicated that the developed barometer-based biosensors have a great potential for applications in point-of-care diagnostics, food safety, and environmental monitoring.

■ ASSOCIATED CONTENT

Supporting Information.

The Supporting Information is available free of charge on the ACS Publications website at DOI: . Experimental details, additional images and tables as presented in the text (PDF)

AUTHOR INFORMATION

Corresponding Author

* Tel: (+86)-20-85227003, E-mail: tyjaq7926@163.com; yuehe.lin@wsu.edu

Notes

The authors declare no competing financial interest.

ACKNOWLEDGMENTS

This work was supported by the National key development program of China (2016YFD0500600), the Technology Research Program of Guangzhou City (201508020100), the Technology Research Program of Guangdong Province (2013B0104104027), and the Guangdong Innovative and Entrepreneurial Research Team Program (201301S-0 105240297). We are grateful for the help provided by Mr. Fangxiang Xu in software programming.

REFERENCES

1. Alsager, O. A.; Kumar, S.; Zhu, B.; Travas-Sejdic, J.; McNatty, K. P.; Hodgkiss, J. M., Ultrasensitive Colorimetric Detection of 17β-Estradiol: The Effect of Shortening DNA Aptamer Sequences. *Anal. chem.* **2015,** *87* (8), 4201-4209.
2. Giljohann, D. A.; Mirkin, C. A., Drivers of biodiagnostic development. *Nature* **2009,** *462* (7272), 461-464.
3. Arlett, J.; Myers, E.; Roukes, M., Comparative advantages of mechanical biosensors. *Nature nanotechnology* **2011,** *6* (4), 203-215.
4. Herzog, F.; Kahraman, A.; Boehringer, D.; Mak, R.; Bracher, A.; Walzthoeni, T.; Leitner, A.; Beck, M.; Hartl, F.-U.; Ban, N., Structural probing of a protein phosphatase 2A network by chemical cross-linking and mass spectrometry. *Science* **2012,** *337* (6100), 1348-1352.
5. Bachar, N.; Liberman, L.; Muallem, F.; Feng, X.; Müllen, K.; Haick, H., Sensor Arrays Based on Polycyclic Aromatic Hydrocarbons: Chemiresistors versus Quartz-Crystal Microbalance. *Acs Applied Materials & Interfaces* **2013,** *5* (22), 11641-11653.
6. Cuddy, M. F.; Poda, A. R.; Brantley, L. N., Determination of Isoelectric Points and the Role of pH for Common Quartz Crystal Microbalance Sensors. *Acs Applied Materials & Interfaces* **2013,** *5* (9), 3514-3518.
7. Lee, M. H.; Thomas, J. L.; Tseng, H. Y.; Lin, W. C.; Liu, B. D.; Lin, H. Y., Sensing of digestive proteins in saliva with a molecularly imprinted poly(ethylene-co-vinyl alcohol) thin film coated quartz crystal microbalance sensor. *Acs Applied Materials & Interfaces* **2011,** *3*(8), 3064-71.
8. Zhu, C.; Yang, G.; Li, H.; Du, D.; Lin, Y., Electrochemical Sensors and Biosensors Based on Nanomaterials and Nanostructures. *Analytical Chemistry* **2015**, 87 (1), 230-249. .
9. de la Escosura‐Muñiz, A.; Baptista‐Pires, L.; Serrano, L.; Altet, L.; Francino, O.; Sánchez, A.; Merkoçi, A., Electrocatalytic Detection: Magnetic Bead/Gold Nanoparticle Double‐Labeled Primers for Electrochemical Detection of Isothermal Amplified Leishmania DNA (Small 2/2016). *Small* **2016,** *12* (2), 204-204.
10. Chen, Z.; Tan, Y.; Xu, K.; Zhang, L.; Qiu, B.; Guo, L.; Lin, Z.; Chen, G., Stimulus-response mesoporous silica nanoparticle-based chemiluminescence biosensor for cocaine determination. *Biosensors and Bioelectronics* **2016,** *75*, 8-14.
11. Ji, X.; Wang, W.; Li, X.; Chen, Y.; Ding, C., Enhanced chemiluminescence detection of Glutathione based on isoluminol-PSM nanoparticles probe. *Talanta* **2016**, 150, 666–670.
12. Borrebaeck, C. A., Antibodies in diagnostics–from immunoassays to protein chips. *Immunology today* **2000,** *21* (8), 379-382.
13. Houseman, B. T.; Huh, J. H.; Kron, S. J.; Mrksich, M., Peptide chips for the quantitative evaluation of protein kinase activity. *Nature biotechnology* **2002,** *20* (3), 270-274.
14. Jia, C.-P.; Zhong, X.-Q.; Hua, B.; Liu, M.-Y.; Jing, F.-X.; Lou, X.-H.; Yao, S.-H.; Xiang, J.-Q.; Jin, Q.-H.; Zhao, J.-L., Nano-ELISA for highly sensitive protein detection. *Biosensors and Bioelectronics* **2009,** *24* (9), 2836-2841.
15. Wang, M.; Sun, C.; Wang, L.; Ji, X.; Bai, Y.; Li, T.; Li, J., Electrochemical detection of DNA immobilized on gold colloid particles modified self-assembled monolayer electrode with silver nanoparticle label. *Journal of pharmaceutical and biomedical analysis* **2003,** *33* (5), 1117-1125.
16. Li, J.; Hong, X.; Li, D.; Zhao, K.; Wang, L.; Wang, H.; Du, Z.; Li, J.; Bai, Y.; Li, T., Mixed ligand system of cysteine and thioglycolic acid assisting in the synthesis of highly luminescent water-soluble CdTe nanorods. *Chemical communications* **2004,** (15), 1740-1741.
17. Wen, W.; Xu, Y.; Zhu, C.; Du, D.; Lin, Y., Recent Advances in Electrochemical Immunosensors. *Analytical Chemistry* **2017**, 89, 138-156.
18. Zhu, C.; Du, D.; Lin, Y., Graphene-like 2D Nanomaterial-Based Biointerfaces for Biosensing Applications. *Biosensors & Bioelectronics* **2017**, 89, 43–55.
19. Zhang, W.; Asiri, A.M.; Liu, D.; Du, D.; Lin, Y., Nanomaterial-based biosensors for environmental and biological monitoring of organophosphorus pesticides and nerve agents. *Trends in Analytical Chemistry* **2014**, 54, 1-10.
20. Bagal-Kestwal, D.; Kestwal, R. M.; Chiang, B. H., Invertase-nanogold clusters decorated plant membranes for fluorescence-based sucrose sensor. *Journal of Nanobiotechnology* **2015,** *13* (1), 1-11.
21. Song, Y.; Luo, Y.; Zhu, C.; Li, H.; Du, D.; Lin, Y., Recent advances in electrochemical biosensors based on graphene two-dimensional nanomaterials. *Biosensors and Bioelectronics* **2016**, 76, 195-212.
22. Rauf, S.; Zhang, L.; Ali, A.; Liu, Y.; Li, J., Label-free Nanopore Biosensor for Rapid and Highly Sensitive Cocaine Detection in Complex Biological Fluids. *ACS Sensors* **2016**, 2 (2), 227–234.
23. Liu, G.; Zhang, K.; Nadort, A.; Hutchinson, M. R.; Goldys, E. M., A Sensitive Cytokine Assay Based on Optical Fibre Allowing Localised and Spatially Resolved Detection of Interleukin-6. *ACS Sensors* **2016**, 2 (2), 218–226.
24. Masson, J.-F., Surface plasmon resonance clinical biosensors for medical diagnostics. *ACS Sensors* **2017,** *2* (1), 16-30.
25. Aube, A.; Charbonneau, D. M.; Pelletier, J. N.; Masson, J.-F. o., Response Monitoring of Acute Lymphoblastic Leukemia Patients Undergoing l-Asparaginase Therapy: Successes and Challenges Associated with Clinical Sample Analysis in Plasmonic Sensing. *ACS Sensors* **2016,** *1* (11), 1358-1365.
26. Lafleur, J. P.; Jönsson, A.; Senkbeil, S.; Kutter, J. P., Recent advances in lab-on-a-chip for biosensing applications. *Biosensors and Bioelectronics* **2016,** *76*, 213-233.
27. Ge, X.; Asiri, A.M., Du, D.; Wen, W.; Wang, S.; Lin, Y., Nanomaterial-enhanced paper-based biosensors. *Trends in Analytical Chemistry* **2014**, 58, 31-39. .
28. Quesada-González, D.; Merkoçi, A., Nanoparticle-based lateral flow biosensors. *Biosensors and Bioelectronics* **2015,** 71, 47–63.

29. Jiang, W.; Liu, Y.; Chen, Y.; Yang, Q.; Chun, P.; Yao, K.; Han, X.; Wang, S.; Yu, S.; Liu, Y., A novel dynamic flow immunochromatographic test (DFICT) using gold nanoparticles for the serological detection of Toxoplasma gondii infection in dogs and cats. *Biosensors and Bioelectronics* **2015,** *72*, 133-139.

30. Watanabe, Y.; Ito, T.; Ibrahim, M. S.; Arai, Y.; Hotta, K.; Phuong, H. V. M.; Hang, N. L. K.; Soda, K.; Yamaoka, M.; Poetranto, E. D., A novel immunochromatographic system for easy-to-use detection of group 1 avian influenza viruses with acquired human-type receptor binding specificity. *Biosensors and Bioelectronics* **2015,** *65*, 211-219.

31. You, Q.; Liu, M.; Liu, Y.; Zheng, H.; Hu, Z.; Zhou, Y.; Wang, B., Lanthanide-Labeled Immunochromatographic Strip Assay for the On-Site Identification of Ancient Silk. *ACS Sensors* **2017**, 2 (4), 569–575.

32. Zhang, L.; Yang, Z.; Sefah, K.; Bradley, K. M.; Hoshika, S.; Kim, M.-J.; Kim, H.-J.; Zhu, G.; Jiménez, E.; Cansiz, S., Evolution of functional six-nucleotide DNA. *Journal of the American Chemical Society* **2015,** *137* (21), 6734-6737.

33. Fu, Q.; Liang, J.; Lan, C.; Zhou, K.; Shi, C.; Tang, Y., Development of a novel dual-functional lateral-flow sensor for on-site detection of small molecule analytes. *Sensors and Actuators B: Chemical* **2014,** *203*, 683-689.

34. Xie, Q.-Y.; Wu, Y.-H.; Xiong, Q.-R.; Xu, H.-Y.; Xiong, Y.-H.; Liu, K.; Jin, Y.; Lai, W.-H., Advantages of fluorescent microspheres compared with colloidal gold as a label in immunochromatographic lateral flow assays. *Biosensors and Bioelectronics* **2014,** *54*, 262-265.

35. Wang, J.; Liu, G.; Wu, H.; Lin, Y., Quantum-dot-based electrochemical immunoassay for high-throughput screening of the prostate-specific antigen . *Small* **2008,** *4*, 82-86.

36. Liu, G.; Lin, Y., Electrochemical quantification of single-nucleotide polymorphisms using nanoparticle probes. *Journal of the American Chemical Society* **129** (34), 10394-10401.

37. Liang, J.; Liu, H.; Lan, C.; Fu, Q.; Huang, C.; Luo, Z.; Jiang, T.; Tang, Y., Silver nanoparticle enhanced Raman scattering-based lateral flow immunoassays for ultra-sensitive detection of the heavy metal chromium. *Nanotechnology* **2014,** *25* (49), 495-501.

38. Fu, Q.; Liu, H. L.; Wu, Z.; Liu, A.; Yao, C.; Li, X.; Xiao, W.; Yu, S.; Luo, Z.; Tang, Y., Rough surface Au@ Ag core–shell nanoparticles to fabricating high sensitivity SERS immunochromatographic sensors. *Journal of Nanobiotechnology* **2015,** *13* (1), 81.

39. Cho, I.-H.; Das, M.; Bhandari, P.; Irudayaraj, J., High performance immunochromatographic assay combined with surface enhanced Raman spectroscopy. *Sensors and Actuators B: Chemical* **2015,** *213*, 209-214.

40. Yang, C.-T.; Pourhassan-Moghaddam, M.; Wu, L.; Bai, P.; Thierry, B., Ultrasensitive detection of cancer prognostic miRNA biomarkers based on surface plasmon enhanced light scattering. *ACS Sensors* **2017**,2 (5), 568–574

41. Neužil, P.; Campos, C.; Wong, C.; Soon, J.; Reboud, J.; Manz, A., From chip-in-a-lab to lab-on-a-chip: towards a single handheld electronic system for multiple application-specific lab-on-a-chip (ASLOC). *Lab on a Chip* **2014,** *14* (13), 2168-2176.

42. Bhatia, S. N.; Ingber, D. E., Microfluidic organs-on-chips. *Nature biotechnology* **2014**, 32, 760-772.

43. Valencia, P. M.; Farokhzad, O. C.; Karnik, R.; Langer, R., Microfluidic technologies for accelerating the clinical translation of nanoparticles. *Nature nanotechnology* **2012,** *7* (10), 623-629.

44. Song, Y.; Zhang, Y.; Bernard, P. E.; Reuben, J. M.; Ueno, N. T.; Arlinghaus, R. B.; Zu, Y.; Qin, L., Multiplexed volumetric bar-chart chip for point-of-care diagnostics. *Nature Communications* **2012,** *3* (4), 187-190.

45. Song, Y.; Xia, X.; Wu, X.; Wang, P.; Qin, L., Integration of Platinum Nanoparticles with a Volumetric Bar‐Chart Chip for Biomarker Assays. *Angewandte Chemie* **2014,** *53* (46), 12451-5.

46. Zhu, Z.; Guan, Z.; Jia, S.; Lei, Z.; Lin, S.; Zhang, H.; Ma, Y.; Tian, Z. Q.; Yang, C. J., Au@Pt Nanoparticle Encapsulated Target‐Responsive Hydrogel with Volumetric Bar‐Chart Chip Readout for Quantitative Point‐of‐Care Testing. *Angewandte Chemie* **2014,** *53* (46), 12503-7.

47. Wu, Z.; Fu, Q.; Yu, S.; Sheng, L.; Xu, M.; Yao, C.; Xiao, W.; Li, X.; Tang, Y., Pt@AuNPs integrated quantitative capillary-based biosensors for point-of-care testing application. *Biosensors and Bioelectronics* **2016,** *85*, 657-663.

48. Zhu, Z.; Guan, Z.; Jia, S.; Lei, Z.; Lin, S.; Zhang, H.; Ma, Y.; Tian, Z. Q.; Yang, C. J., Au@ Pt Nanoparticle Encapsulated Target-Responsive Hydrogel with Volumetric Bar-Chart Chip Readout for Quantitative Point-of-Care Testing. *Angewandte Chemie International Edition* **2014,** *53* (46), 12503-12507.

49. McKee, D., Catalytic decomposition of hydrogen peroxide by metals and alloys of the platinum group. *Journal of Catalysis* **1969,** *14* (4), 355-364.

50. Tao, Y.; Ma, Y.; Huang, Q.; He, M.; Cao, G.; Xia, S.; Zhang, D.; Wang, M.; Hong, Z.; Tong, Z., High Durable Ternary Nanodendrites as Effective Catalysts for Oxygen Reduction Reaction. *Acs Applied Materials & Interfaces* **2016**, 8 (36), pp 23646–23654.

51. Fu, S.; Zhu, C.; Song, J.; Engelhard, M. H.; Xia, H.; Du, D.; Lin, Y., PdCuPt Nanocrystals with Multi-branches for Enzyme-free Glucose Detection. *Acs Applied Materials & Interfaces* **2016**, 8 (34), 22196–22200.

52. Luo, M.; Lu, P.; Yao, W.; Huang, C.; Xu, Q.; Wu, Q.; Kuwahara, Y.; Yamashita, H., Shape and Composition Effects on Photocatalytic Hydrogen Production for Pt-Pd Alloy Cocatalysts. *Acs Applied Materials & Interfaces* **2016**, 8 (32), 20667–20674 .

53. Xue, H.; Tang, J.; Gong, H.; Guo, H.; Fan, X.; Wang, T.; He, J.; Yamauchi, Y., Fabrication of PdCo Bimetallic Nanoparticles Anchored on Three-Dimensional Ordered N-Doped Porous Carbon as an Efficient Catalyst for Oxygen Reduction Reaction. *Acs Applied Materials & Interfaces* **2016,** 8 (32), 20766–20771.

54. Ataee-Esfahani, H.; Wang, L.; Nemoto, Y.; Yamauchi, Y., Synthesis of bimetallic Au@ Pt nanoparticles with Au core and nanostructured Pt shell toward highly active electrocatalysts. *Chemistry of Materials* **2010,** *22* (23), 6310-6318.

55. Zan, X.; Fang, Z.; Wu, J.; Xiao, F.; Huo, F.; Duan, H., Freestanding graphene paper decorated with 2D-assembly of Au@ Pt nanoparticles as flexible biosensors to monitor live cell secretion of nitric oxide. *Biosensors and Bioelectronics* **2013,** *49*, 71-78.

56. ‡, Z. Z.; ‡, Z. G.; ‡, S. J.; Lei, Z.; Lin, S.; Zhang, H.; Ma, Y.; Tian, Z. Q.; Yang, C. J., Au@Pt Nanoparticle Encapsulated Target-Responsive Hydrogel with Volumetric Bar-Chart Chip Readout for Quantitative Point-of-Care Testing †. *Angewandte Chemie International Edition* **2014,** *53* (46), 12711–12715.

57. Fu, Q.; Wu, Z.; Xu, F.; Li, X.; Yao, C.; Xu, M.; Sheng, L.; Yu, S.; Tang, Y., A portable smart phone-based plasmonic nanosensor readout platform that measures transmitted light intensities of nanosubstrates using an ambient light sensor. *Lab on A Chip* **2016,** *16* (10).

58. WANG, S.; LIANG, G.-d.; LI, Z.-l.; XIAO, Y.-h.; HUANG, C.-g., Pollution status and risk assessment of lean meat powder in pork in Wuhan in 2011 [J]. *Chinese Journal of Health Laboratory Technology* **2012,** *5*, 078.

59. Wei, W.; Ling-Yun, J., Progress in aptamer screening methods. *Chinese Journal of Analytical Chemistry* **2009,** *37* (3), 454-460.

60. Wang, Y.; Zhang, Y.; Yan, T.; Fan, D.; Du, B.; Ma, H.; Wei, Q., Ultrasensitive electrochemical aptasensor for the detection of thrombin based on dual signal amplification strategy of Au@GS and DNA-CoPd NPs conjugates. *Biosensors & Bioelectronics* **2016,** *80* (65), 11-30.

61. Yue, Q.; Shen, T.; Lei, W.; Xu, S.; Li, H.; Xue, Q.; Zhang, Y.; Gu, X.; Zhang, S.; Liu, J., A convenient sandwich assay of thrombin in biological media using nanoparticle-enhanced fluorescence polarization. *Biosensors & Bioelectronics* **2014,** *56* (56), 231-236.

62. He, S.-B.; Wu, G.-W.; Deng, H.-H.; Liu, A.-L.; Lin, X.-H.; Xia, X.-H.; Chen, W., Choline and acetylcholine detection based on peroxidase-like activity and protein antifouling property of platinum nanoparticles in bovine serum albumin scaffold. *Biosensors and Bioelectronics* **2014,** *62*, 331-336.

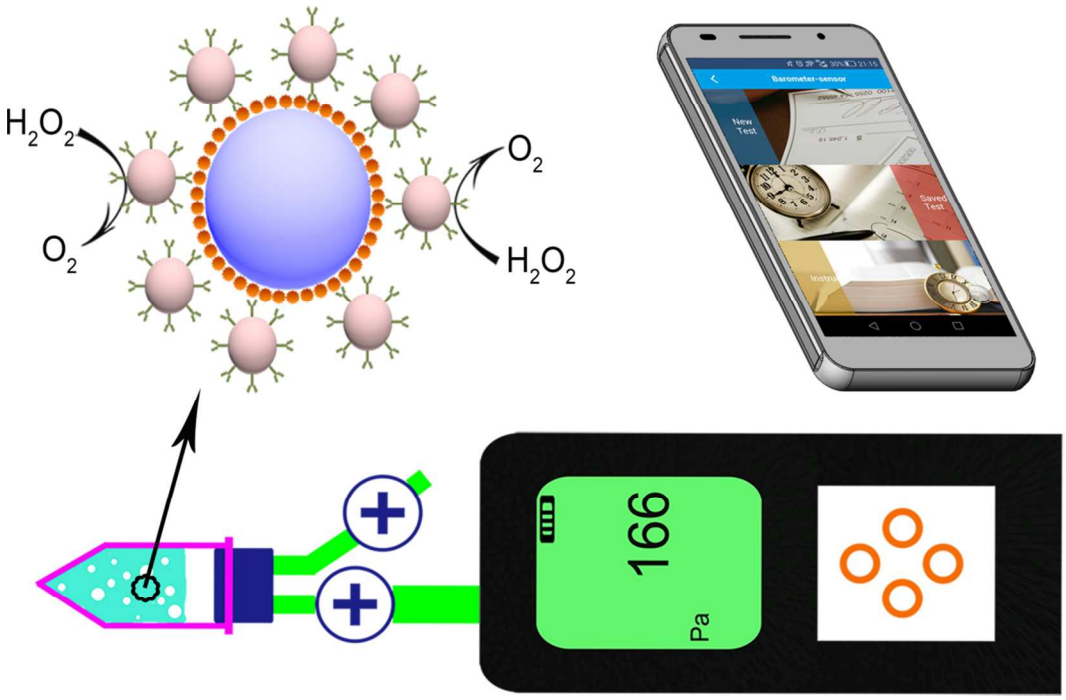
H_2O_2
O_2
O_2
H_2O_2
Barometer-sensor
New Test
Saved Test
166
Pa

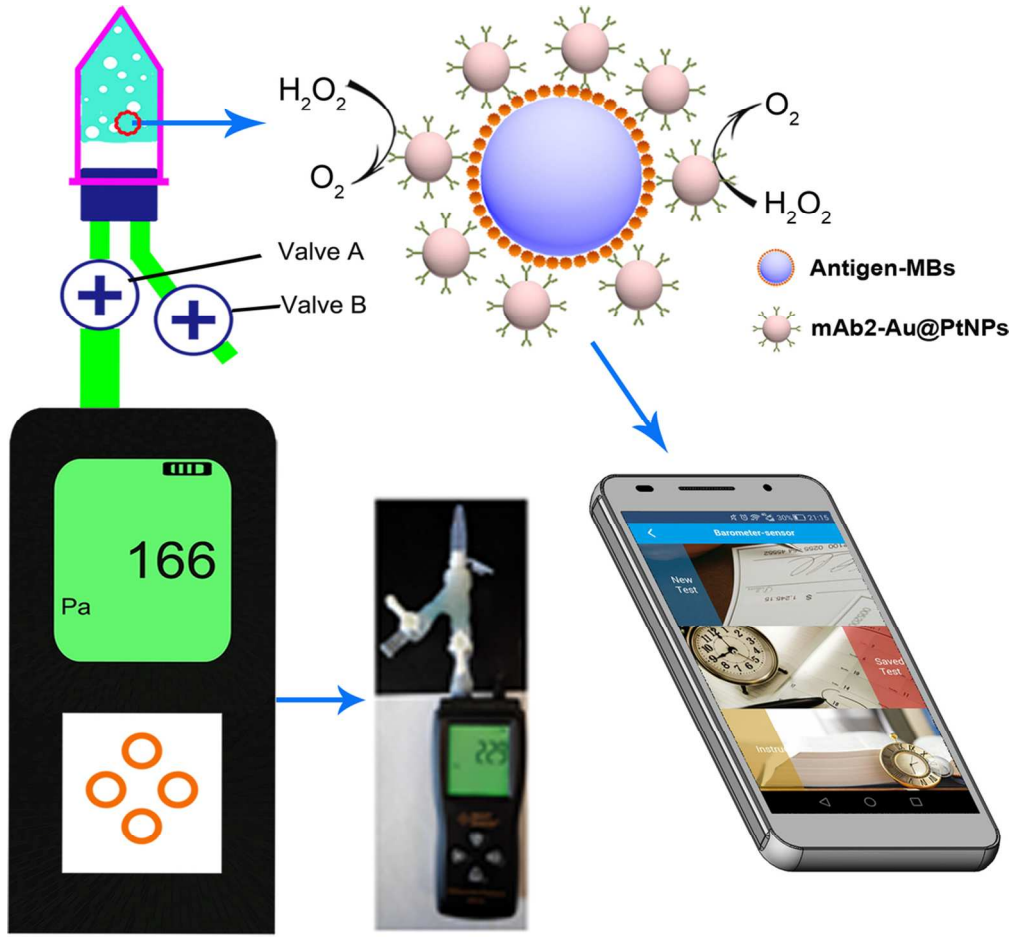

Scheme of the barometer-based biosensor. This barometer-based biosensor operates based on the measurement of oxygen generation in a limited chamber by using a precise barometer. The design employs Au@PtNPs as probes for the decomposition of H2O2 to release O2. The generated O2 accumulates within the limited volume chamber and causes an increase in pressure, which is measured by a portable barometer. Analyte concentrations are linearly proportional to the measured pressures.

51x48mm (600 x 600 DPI)